LANGMUIR
Article
Cite This: *Langmuir* 2019, 35, 12326−12338
pubs.acs.org/Langmuir

Comprehensive Study of the Liquid Expanded−Liquid Condensed Phase Transition in 1,2-Dimyristoyl-*sn*-glycero-3-phospho-L-serine Monolayers: Surface Pressure, Volta Potential, X-ray Reflectivity, and Molecular Dynamics Modeling

Yu. A. Ermakov,[*,†] V. E. Asadchikov,[‡] B. S. Roschin,[‡] Yu. O. Volkov,[‡,§] D. A. Khomich,[∥,⊥] A. M. Nesterenko,[*,#,∇] and A. M. Tikhonov[*,§,○]

[†]Frumkin Institute of Physical Chemistry and Electrochemistry, Russian Academy of Sciences, Leninsky pr., 31/4, Moscow 119071, Russia

[‡]Shubnikov Institute of Crystallography, Federal Research Center Crystallography and Photonics, Russian Academy of Sciences, Leninsky pr., 59, Moscow 119333, Russia

[§]Institute of Solid State Physics, Russian Academy of Sciences, Academician Ossipyan str. 2, Moscow District, Chernogolovka 142432, Russia

[∥]Lomonosov Moscow State University, Biology Faculty, Leninskie gory 1/12, Moscow 119234, Russia

[⊥]Engelhardt Institute of Molecular Biology, Russian Academy of Sciences, Vavilova, 32, Moscow 119991, Russia

[#]Belozersky Institute of Physico-Chemical Biology, Lomonosov Moscow State University; Leninskie gory 1/40, Moscow, 119991, Russia

[∇]Shemyakin-Ovchinnikov Institute of Bioorganic Chemistry, Russian Academy of Sciences, Miklukho-Maklaya 16/10, Moscow 117997, Russia

[○]Kapitza Institute for Physical Problems, Russian Academy of Sciences, ul. Kosygina 2, Moscow 119334, Russia

Supporting Information

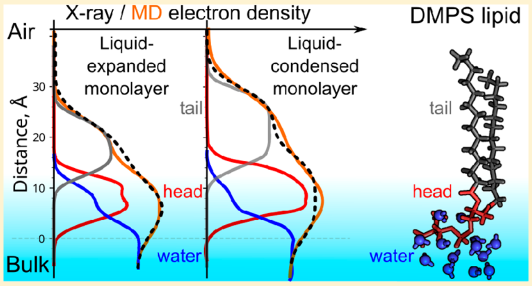

ABSTRACT: An integrated approach is applied to reveal fine changes in the surface-normal structure of 1,2-dimyristoyl-*sn*-glycero-3-phospho-L-serine (DMPS) monolayers at the air−lipid−water interface occurring in a liquid expanded (LE)−liquid condensed (LC) transition. The combination of the Langmuir monolayer technique, X-ray reflectometry, and molecular dynamics (MD) modeling provides new insight into the molecular nature of electrostatic phenomena in different stages of lipid compression. A homemade setup with a laboratory X-ray source ($\lambda = 1.54$ Å) offers a nondestructive way to reveal the structural difference between the LE and LC phases of the lipid. The electron density profile in the direction normal to the interface is recovered from the X-ray reflectivity data with the use of both model-independent and model-based approaches. MD simulations of the DMPS monolayer are performed for several areas per lipid using the all-atom force field. Using the conventional theory of capillary waves, a comparison is made between the electron density profiles reconstructed from the X-ray data and those calculated directly from MD modeling, which demonstrates remarkable agreement between the experiment and simulations for all selected lipid densities. This confirms the validity of the simulations and allows an analysis of the contributions of the hydrophobic tails and hydrated polar groups to the electron density profile and to the dipole component of the electric field at the interface. According to the MD data, the dependence of the Volta potential on the area per lipid in the monolayer has a different molecular nature below and above the phase transition. In the LE state of the monolayer, the potential is determined mostly by the oriented water molecules in the polar region of the lipid. In the LE−LC transition, these molecules are displaced to the bulk, and their effect on the Volta potential becomes insignificant compared with the contribution of the hydrophobic tails. The hydrophobic tails are highly ordered in the state of the liquid crystal so that their dipole moments entirely determine the growth of the potential upon compression up to the monolayer collapse.

INTRODUCTION

Langmuir monolayers consisting of phospholipids are commonly used as model systems in various types of studies of the structural aspects of the interaction of miscellaneous substances

Received: May 15, 2019
Revised: August 24, 2019
Published: September 3, 2019

DOI: 10.1021/acs.langmuir.9b01450
Langmuir 2019, 35, 12326−12338

with the surface of cell membranes.[1,2] These studies are directed to improve biomedical applications, for instance, by solving the drug delivery problem or to control the membrane activity of a large number of substances developed for pharmacologic purposes. It was revealed that the adsorption of inorganic ions and foreign molecules at the surface of a cell membrane and their subsequent incorporation into the hydrophobic core of the membrane together with the associated water molecules leads to a total reorganization of the lipid−water interface. Cluster and domain formation in monolayers is the most apparent result of this phenomenon, as detected by fluorescent and Brewster angle microscopy[3−6] and supported by molecular dynamics (MD) simulations.[7,8] The experimental basis for lipid clustering in membranes is related to a fundamental property of the phospholipids revealed in liquid−solid transitions, which are particularly well pronounced in Langmuir monolayers of saturated lipids, such as dipalmitoylphosphatidylcholine (DPPC) and 1,2-dimyristoyl-*sn*-glycero-3-phospho-L-serine (DMPS).[9−11] Many authors have proposed quantitative models of a liquid expanded (LE)−liquid condensed (LC) phase transition assuming equilibrium between free- and cluster-associated lipid molecules.[12−14] However, these models disregard the electrostatic input to the phase transition phenomenon, and there are no MD simulations known in the literature concerning the molecular nature of the related electrostatic effects. The electrostatic effects seem to be especially significant for negatively charged anionic lipids, such as DMPS. Previously, we found that the electric field at the lipid−water interface, namely, the dipole component of the boundary potential, is extremely sensitive to the packing of phosphatidylserine (PS) molecules in membranes.[15] Later, this result helped us to explain the significant modulations of biomembrane activity induced by inorganic multivalent cations with a high affinity to the PS moiety.[16] Our most reasonable interpretation of these results suggested a direct relation between the dipole component and the lipid reorganization of the biomembranes caused by the lateral condensation of the PS molecules. However, the process of the condensation at the molecular level has remained unclear until now. This prompted us to concretize this idea, having studied in detail the molecular nature of electrostatic phenomena arising during the phase transition in DMPS monolayers, which are recorded by the Langmuir method, monitored by measuring the reflectivity of X-rays, and simulated by MD methods.

MD methods have been widely used in lipid monolayer research since the 1990s[17,18] without any significant transformations. Thus far, MD methods have been applied mostly to monolayers of zwitterionic molecules. The LE−LC phase transitions and hexagonal ordering occurring, for example, in a DPPC monolayer, were successfully simulated in two independent all-atom MD studies.[19,20] Coarse-grained approaches are also often used for similar systems.[21] It is important to note that MD methods have allowed one to study the changes in the electric potential distribution accompanied by DPPC monolayer compaction.[22] We found only one example of an application of the MD method to monolayers of anionic lipids,[23] although there were no details regarding electrostatic phenomena. Therefore, we focus on the electrostatic potentials in monolayers of a negatively charged DMPS lipid. In addition, we verify our MD calculations by comparing the results with electron density distributions reconstructed from X-ray reflectivity obtained for the same systems.

X-ray surface scattering methods offer direct ways to probe the essential details of the molecular structure at the lipid−water interface,[24−26] including the geometrical parameters of packed lipids and their hydration shells.[26−29] In particular, synchrotron X-ray reflectometry applied to a monolayer system of neutral molecules allows the detection of a significant difference in lipid packing in the LE and LC states.[30] This method also facilitates the detection of subtle structural changes in the lipid layer accompanied by an LE−LC transition.[31−34] Admittedly, the direct use of a high-intensity beam of ionizing synchrotron radiation in the experiment can cause burns in a monolayer, especially when it contains unsaturated molecules. Indeed, X-ray damage of monolayer samples was detected for heavy irradiation of DMPS and neutral phosphocholines with an unsaturated hydrocarbon chain at an air−water interface and was studied by Danauskas et al.[35] as a model system for radiation defects in natural cell membranes. In refs 36 and 37, the authors demonstrated an experimental method of how to avoid radiation damage to complex protein−phospholipid films using a sample cell filled with ^{4}He gas.

Alternatively, a laboratory apparatus equipped with an anode tube as an X-ray source is very attractive for such reflectometry experiments. Although, in general, an anode tube provides a less intense photon beam than a synchrotron source, the spatial resolution of the data collected by the diffractometer is still quite comparable to that obtained previously at a synchrotron-based installation.[38] Our preliminary studies of DMPS monolayers have demonstrated the potential of this rather gentle and nondestructive method to reveal the difference between the LE and LC structures of this lipid.

In this paper, we carry out a comprehensive study of the LE−LC phase transition in DMPS monolayers by combining, for the first time, the Langmuir monolayer technique, X-ray reflectometry, and MD modeling. The molecular dynamics simulations allow us to determine the role of oriented water molecules in the LE−LC phase transition while measurements of X-ray reflectivity and Volta potential serve as the basis for testing the simulation results. Detailed analysis of the calculated positions of the atoms of both DMPS and H_2O molecules shows that in the LE state of the monolayer the total boundary potential is determined mainly by oriented water molecules in the polar region of the lipid. In the LE−LC transition, these molecules are displaced into the bulk so that their effect on the Volta potential becomes insignificant compared with the contribution of the hydrophobic tails. Since the hydrophobic tails are highly ordered in the state of the liquid crystal, their dipole moments entirely determine the growth of the potential upon compression up to the monolayer collapse.

■ MATERIALS AND METHODS

Monolayer Measurements. In the monolayer sample preparation, we used DMPS (1,2-dimyristoyl-*sn*-glycero-3-phospho-L-serine, Avanti Polar Lipids) that was dissolved up to 0.5 mg/mL in a chloroform−methanol (5:1, v/v) mixture (Merck KGaA and Macron Fine Chemicals, respectively). A film of the lipid was applied by a Hamilton syringe on the surface of a 100 mM KCl (Sigma-Aldrich) solution in water that was distilled three times. Pressure (π)−area (A) diagrams and the Volta potential were measured simultaneously by MicroTrough XS, version 4.0 (Kibron Inc.), with the PTFE trough and two POM barriers. The cleaning procedure was repeated and checked to ensure that the pressure and potential were stable to within 0.1 mN/m and 10 mV for the maximal range of area available in the trough. When a lipid film was applied and dried (approximately 20 min at room temperature of approximately 20 °C), the measurements started with a compression speed of 10 mm/min (approximately ~7 Å^2 per molecule/min). The typical reproducibility of the π-area diagram was approximately 1−3%.

X-ray Measurements. Samples of DMPS phospholipid monolayers were studied in an airtight cell with X-ray-transparent windows by the technique described in refs 39 and 40. The monolayers were prepared by spreading a calculated volume of a phospholipid solution (0.5 mg/mL in a 5:1 chloroform−methanol mixture) with the use of a Hamilton syringe over the surface of a liquid substrate (pH ≈ 7, 100 mM KCl) placed in a fluoroplastic dish (Teflon) with a diameter D of 100 mm. Thus, we obtained a set of samples with various values of the area per molecule corresponding to different lipid phase states of the monolayer (see Figure 1 and Table 1). In the experiment, the nominal area per molecule is determined by the ratio of the deposited amount of DMPS to the area of the dish. To achieve the most tight packing of the lipid in the monolayer, we prepared two samples in the immediate vicinity of the collapse of the monolayer (*nominal* areas per molecule are 37 and 41 Å^2).

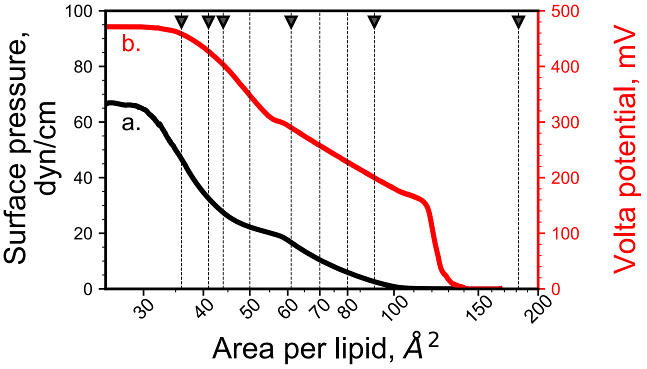

Figure 1. Compression plots of the surface pressure (a) and Volta potential (b) measured for the DMPS monolayer for 100 mM KCl in the bulk of water. The vertical dotted lines specify the areas used in the MD simulations; the triangles correspond to the areas selected for the X-ray measurements. The abscissa in the figure is transformed hyperbolically to reveal the linear dependence of the potential on the inverted density.

The transverse structure of the lipid monolayer was investigated with X-ray reflectometry using a versatile homemade diffractometer equipped with a movable emitter−detector system.[41] In the setup, an X-ray tube with a copper anode was used as the emitter. The $K_{\alpha 1}$ line (photon energy $E = 8048$ eV, wavelength $\lambda = 1.5405 \pm 0.0001$ Å) was chosen from the tube emission spectrum using a single reflection Si(111) crystal monochromator. The three-slit collimation system forms a probing beam in the plane of incidence with an angular width of ~10^{-4} rad. The vertical and horizontal beam sizes are ~0.1 and 8 mm, respectively. The angular resolution of the point detector $2\Delta\beta \approx 1.7 \times 10^{-3}$ rad is determined by the entrance slit with a gap of 1 mm at a distance of ~570 mm from the sample's center. To reduce the beam's absorption and scattering in the air, we used vacuum paths with X-ray-transparent windows.

Let $\mathbf{k}_{\text{in}}$ and $\mathbf{k}_{\text{sc}}$ be the wavevectors with an amplitude $k_0 = 2\pi/\lambda$ for the incident and scattered beams, respectively (Figure 2, left). It is useful to introduce a coordinate system in which the origin O lies at the center of the illumination region, the xy plane coincides with the water boundary, the x-axis is perpendicular to the beam direction, and the z-axis is directed along the normal to the surface opposite to the force of gravity. The specular reflectivity, R, was measured as a function of the wavevector transfer $\mathbf{q} = \mathbf{k}_{\text{sc}} - \mathbf{k}_{\text{in}}$ component normal to the water surface, $q_z = (4\pi/\lambda)\sin\alpha$, by varying the incident angle, α, in the plane of incidence, xz, while keeping the scattering angle fixed at $\beta = \alpha$. Note that $R \approx 1$ at grazing angles $\alpha < \alpha_c$, where α_c is the angle of the total external reflection for the water surface. The critical angle is given by the volume electron density in water $\rho_w \approx 0.333$ e$^-$/Å^3 so that $\alpha_c = \lambda\sqrt{r_e\rho_w/\pi} \approx 0.15°$, where $r_e = 2.814 \times 10^{-5}$ Å is the electron's Thompson scattering length.

MD Simulations. Simulations were performed using the all-atom force field CHARMM36 with the GROMACS 5.1.4/2018 package.[42] The DMPS molecules were in the same ionic state: the phosphate and carboxyl groups were deprotonated, and the amino groups were protonated. The background electrolyte concentration was the same as in the experiments (100 mM KCl). The bonds with hydrogen were constrained, and the integration step was 2 fs. To simulate monolayer conditions, we formed a normal lipid bilayer and inserted the vacuum part into the interlayer plane. This method was introduced in recent studies of similar systems.[43] The system was treated as periodic with two monolayers separated by bulk water from one side and by vacuum from another side (Figure 3). All simulations were performed in an NVT ensemble, keeping the surface constant. In fact, the volume of the whole system was restricted, but its "liquid" part had no restrictions due to the presence of the vacuum layer. Since the z-component of the pressure tensor is the constant reference value, one can refer to our conditions as an "NSP$_z$T ensemble", indicating that the monolayer surface is fixed and the z-component of the pressure tensor is zero. We verified our results in NPT simulations fixing the system height and using the lateral pressure value measured in the corresponding NVT system as a reference for the lateral pressure.

A full list of the simulated systems with DMPS monolayers is presented in Table S1. In most cases, these systems consisted of 50 lipids per monolayer. However, to verify some of the results, we used two systems with four times more DMPS molecules. The water−vacuum interface was simulated separately as the reference system that

Table 1. Estimates of the Two-Layer Model Parameters for the DMPS Monolayers in Equation A1 (See Also Figure 2 right), MD Data, and Comparison between the Roughness Root Mean Square Heights[a]

monolayer		head group region				hydrophobic tail region				roughness		
A (Å^2)	$\Pi(A)$ (mN/m)	L_1 (Å)	ρ_1/ρ_w	n	n^*	L_2 (Å)	ρ_2/ρ_w	L_2^* (Å)	ρ_2^*/ρ_w	σ_{fit} (Å)	σ_0 (Å)	σ_{eff} (Å)
181	~1	$14^{\pm 2}$	$1.18^{\pm 0.02}$	$81^{\pm 8}$	$74.5^{\pm 0.9}$	$7.0^{\pm 0.3}$	$0.48^{\pm 0.07}$	$11^{\pm 1}$	$0.36^{\pm 0.04}$	$2.6^{\pm 0.5}$	$2.6^{\pm 0.1}$	$2.6^{\pm 0.2}$
91	3	$14^{\pm 2}$	$1.21^{\pm 0.04}$	$31^{\pm 3}$	$25.5^{\pm 0.4}$	$8.6^{\pm 0.6}$	$0.72^{\pm 0.04}$	$9^{\pm 1}$	$0.71^{\pm 0.06}$	$2.7^{\pm 0.5}$	$2.7^{\pm 0.1}$	$2.6^{\pm 0.2}$
61	17	$14^{+2/-1}$	$1.24^{\pm 0.02}$	$13^{\pm 1}$	$14.5^{\pm 0.6}$	$10.5^{\pm 0.6}$	$0.80^{\pm 0.02}$	$11.5^{\pm 0.6}$	$0.87^{\pm 0.08}$	$2.8^{\pm 0.5}$	$2.8^{\pm 0.1}$	$2.8^{\pm 0.2}$
45	25	$14^{\pm 1}$	$1.30^{\pm 0.02}$	$6.8^{\pm 0.7}$	$7.3^{\pm 0.4}$	$13.3^{\pm 0.6}$	$0.93^{\pm 0.02}$	$13.5^{\pm 0.5}$	$1.00^{\pm 0.09}$	$3.3^{\pm 0.5}$	$3.2^{\pm 0.1}$	$2.9^{\pm 0.2}$
41	30	$13^{\pm 1}$	$1.38^{\pm 0.03}$	$3.3^{\pm 0.3}$	$5.8^{\pm 0.3}$	$14.8^{\pm 0.5}$	$0.88^{\pm 0.2}$	$15.1^{\pm 0.8}$	$0.99^{\pm 0.09}$	$3.9^{\pm 0.5}$	$3.5^{\pm 0.1}$	$3.2^{\pm 0.2}$
A_C	45	$12^{\pm 1}$	$1.42^{\pm 0.03}$	$2.6^{\pm 0.3}$		$15.1^{\pm 0.5}$	$0.94^{\pm 0.02}$			$4^{\pm 1}$	$4.0^{\pm 0.1}$	$3.2^{\pm 0.2}$

[a] A is the area per lipid molecule. $\Pi(A)$ is the surface pressure (see Figure 1). L_1 and L_2 are the thicknesses of the head group and acyl group regions, respectively; ρ_1 and ρ_2 represent the average electron densities of the head group and acyl group regions, respectively. Roughness: σ_{fit} is the fitting parameter of the two-layer model; σ_0 is calculated from the capillary waves formula (A3); σ_{eff} is estimated by convolving the MD electron density profiles (eq 2). n is the average number of water molecules per lipid molecule obtained from the parameter values for the two-layer model (see Appendix I). For MD data, n^* is the average number of water molecules in the head group region per lipid calculated from the contribution of water to the electron density profile (Figure 6, blue curves), and ρ_2^* and L_2^* are the parameters calculated from the contribution of the hydrophobic part of the lipid to the electron density profile (Figure 6, gray curves). The electron densities are normalized to $\rho_w = 3.33 \times 10^{29}$ e$^-$/m^3.

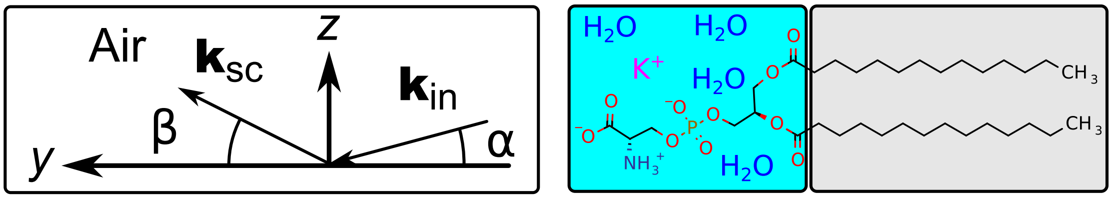

Figure 2. Kinematics of the X-ray scattering at the water−air interface (left) and chemical structure of the ionized DMPS molecule (right) with the colored cyan and gray blocks indicating the polar and hydrophobic parts, respectively, as postulated in the model-based approach.

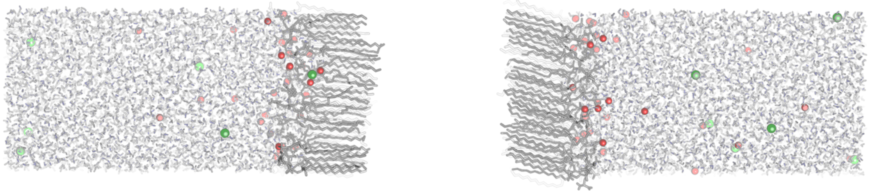

Figure 3. Structure of the scene used for the simulation of two similar DMPS monolayers separated by vacuum. The co-ions Cl^- and counterions K^+ are shown by green and red spheres, respectively.

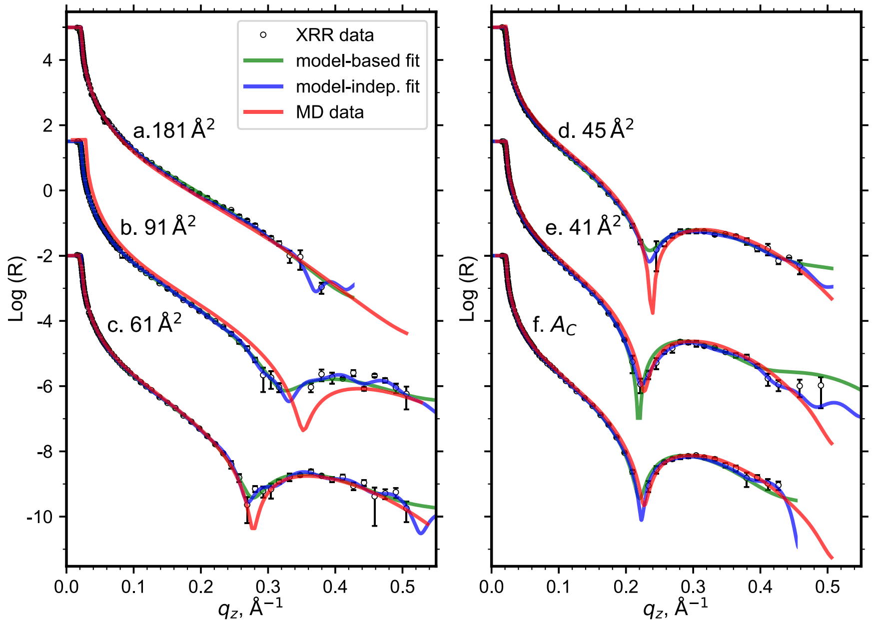

Figure 4. X-ray experimental data (open circles) and the calculated function $R(q_z)$ for the model-based (green line) and model-independent (blue line) approaches plotted with the convolved MD results (red line) for monolayers with different areas per lipid, which correspond to the triangles in Figure 1. The red lines for the data sets e (A = 41 Å^2) and f ($A = A_C$) are the same and correspond to MD at 41 Å^2.

is necessary for the potential calculations. MD trajectories were analyzed in their equilibrium section (250−500 ns). The electron density, potential, and water orientation parameters were averaged in 10 ns intervals and then used for subsequent statistical analysis. Some of the scripts developed for trajectory processing were deposited at GitHub (https://github.com/comcon1/mdantools). These Python scripts utilize the MDAnalysis library[44] and standard matplotlib/numpy libraries.

We estimate the first and the second-order parameters with the following slab and ensemble averages: $1/2\langle\cos\Psi\rangle$ and $1/2\langle 3\cos^2\Psi - 1\rangle$, where Ψ is the angle between the dipole moment of H_2O and the direction opposite to the z-axis (see Figure 2, left). To visualize the different phase states of the monolayer, we used triangulated network images, presented in Figure S2 and Videos S1, S2, and S3. Every circle in these images corresponds to the center of mass of the C4−C9 section of the acyl chain. The edges were drawn by the Delaunay triangulation algorithm. All of the construction scripts were made with MD analysis and numpy/scipy libraries and were also deposited at GitHub (*lipidnet* folder at https://github.com/comcon1/mdantools). All of the 3D images were made using PyMOL software (Schrodinger LLC, PyMOL). We additionally used VMD software to visually handle the trajectories.[45] The electrostatic potential was calculated with twice the integration of the charge density by the Poisson equation. The profiles of the electrostatic potential and water order parameters were plotted as functions of distance to the average plane of the phosphorus atoms. The same approach was used in our recent studies of water orientation at a lipid surface.[46] To compare the X-ray and MD data in the figures below, we set the position of the interface between the head group block (Figure 2, right) and the water bulk as a zero in the interfacial depth axis.

RESULTS AND DISCUSSION

The experimental curves for the DMPS monolayer shown in Figure 1 demonstrate the typical shape for the LE−LC transition in both the pressure−area diagram (a) and Volta potential (b). It should be emphasized that the experimental points with nominal area per molecule less than 40 Å^2 do not correspond to a monolayer with such low A due to the phenomenon of collapse.

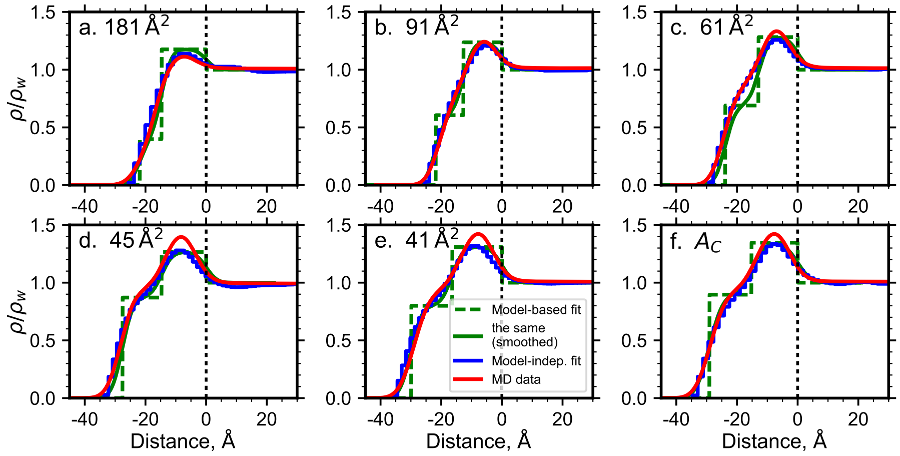

Figure 5. Electron density profiles, $\rho(z)$, obtained from the experimental reflectivity data with the model-based (green, dashed is for $\sigma_0 \equiv 0$) and model-independent (blue) approaches and those calculated by the convolved MD distributions (red). The red lines for the data sets e ($A = 41$ Å^2) and f ($A = A_C$) are the same and correspond to MD at 41 Å^2. The zero at the abscissa axis corresponds to the boundary between the outer plane of the head group slab and the water surface (see Figure 2). Estimates of the parameters of the two-layer model are displayed in Table 1.

Moreover, the exact value of area, A_C, at the collapse is not known, since it is very sensitive to experimental conditions, such as materials of the trough and barriers, compression procedures, salt contaminations, uncertainties in bulk concentrations, etc. Therefore, the lipid concentrations selected for X-ray measurements (triangles, Figure 1) are overestimated near the collapse. In the X-ray experiment, we intentionally studied one system in the state of collapse (with *nominal* area per lipid of 37 Å^2) in ensure maximum surface packing density of the lipid ($A = A_C$).

Previously, we found a direct proportionality between the increment of the Volta potential and pressure with a compression applied to the monolayer at various experimental conditions including the phase transition section.[47] The present study is focused on the molecular nature of these phenomena determined by X-ray data and MD simulated structures.

X-ray Reflectivity Analysis. The experimental reflectivity data presented in Figure 4 by circles were analyzed by applying two different approaches. The first approach employs a general expression derived from the distorted wave Born approximation (DBWA) for X-ray scattering (see X-ray kinematics in Figure 2, left) that relates the reflectivity to the electron density gradient normal to the interface, $\mathrm{d}\langle\rho(z)\rangle/\mathrm{d}z$, averaged over the interfacial plane[48] by the following equation:

$$R(q_z) \approx \left|\frac{q_z - q_z^t}{q_z + q_z^t}\right|^2 \left|\frac{1}{\rho_w}\int_{-\infty}^{+\infty}\left\langle\frac{\mathrm{d}\rho(z)}{\mathrm{d}z}\right\rangle \exp\left(i\sqrt{q_z q_z^t}\, z\right)\mathrm{d}z\right|^2 \quad (1)$$

where $q_z' = \sqrt{q_z^{\,2} - q_c^{\,2}}$ and $q_c = 2k_0 \sin\alpha_c \approx 0.022$ Å^{-1}. Details of the calculations are described in Appendix I. Earlier, we utilized this method in data analysis for various experimental systems with adsorption films on solid substrates and the surfaces of colloidal solutions and at air−water and oil−water interfaces.[26,49−52]

In the case under consideration, to achieve good agreement between the model curves and the experimental data, it is sufficient to divide the interface structure into two layers. In accordance with the structure of the DMPS molecule, the first layer of thickness L_1 and electron density ρ_1 is formed by the polar PS groups, while the second layer of thickness L_2 and electron density ρ_2 is formed by the aliphatic tails $-C_{13}H_{27}$ (see Figure 2, right). The MD simulations and quantitative analysis of this system numerically confirm the validity of such parametrization for the monolayer structure. The fitted parameters of this model are listed below in Table 1.

The second approach is based on the extrapolation of the asymptotic behavior of the reflectivity curve to a range of large values of q_z with no a priori assumptions regarding the sample's structure.[38,53,54] The model-independent approach provides the distribution of the electron density, which is used as a reference for the structural model, while the model-based approach allows us to quantitatively estimate the parameters for the structural components of a lipid layer. The simultaneous application of these two independent approaches in the reflectivity data analysis considerably reduces the ambiguity of the solutions for the electron density profiles.

In the experiment, part of the reflected intensity is lost due to diffuse scattering by thermally excited surface capillary waves of water.[53−57] On one hand, the fraction of the capillary roughness spectrum that contributes to the diffuse scattering is limited by the angular resolution of the detector's slits, $2\Delta\beta$. Since in our experiments $2\Delta\beta \approx 1.7$ mrad, the lower spatial frequency cutoff is $Q_{\min} = q_z^{\max}\Delta\beta \sim 5 \times 10^{-4}$ Å^{-1}, which corresponds to an in-plane length of $2\pi/Q_{\min} \sim 10^3$ nm. On the other hand, the linear size of a simulated cell in the MD simulations does not exceed $C \sim 5$ nm ($2\pi/C \approx 0.1$ Å^{-1}). Thus, the MD simulations do not correctly account for the capillary wave roughness, which is apparent in the reflectivity.

Assuming that the capillary wave fluctuations at the water−lipid and lipid−air interfaces are completely correlated along the z-axis normal to the surface (i.e., they are conformal), their effect on the profiles $\rho_{\mathrm{calc}}(z)$ calculated by MD can be estimated with the use of a linear convolution of the profiles with a one-dimensional statistical height−height correlation function, which in our case is a Gaussian distribution.

$$\rho(z) = \int_{-\infty}^{+\infty} \frac{\rho_{\mathrm{calc}}(z')}{\sigma_{\mathrm{eff}}\sqrt{2\pi}} \exp\left[-\left(\frac{z - z'}{\sigma_{\mathrm{eff}}\sqrt{2}}\right)^2\right]\mathrm{d}z' \quad (2)$$

The values for the roughness parameter, σ_{eff}, were estimated by a numerical fit based on the discrepancy between the experimental reflectivity curves, $R(q_z)$, and the curves calculated by the MD profiles, $\rho_{\mathrm{calc}}(z)$, with the use of eq 1. Comparisons between the fitted values, σ_{eff}, and the theoretical values, σ_0,

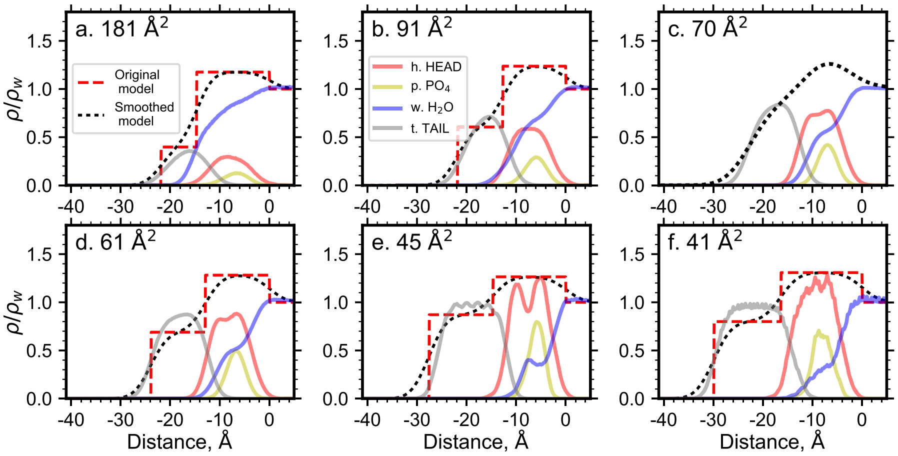

Figure 6. Contributions of four molecular subsystems to the electron density profile: hydrocarbon tails (t), polar head groups (h), and the phosphate (p) and water molecules (w). The raw electron density was obtained with the model-based approach (red dashes) and after smoothing (black dots). The zero at the abscissa axis corresponds to the boundary between the outer plane of the head group block and the water surface. The separation of the lipid molecule into the head and tail parts is depicted in Figure 2 (right).

calculated from the surface tension data according to eq A3 are listed in Table 1.

We note that the actual roughness height distribution may deviate from a Gaussian distribution and the roughnesses of the lipid layer interfaces (water−head groups, head groups−alkyl chains−$C_{13}H_{27}$, and air−chains) may not be strictly conformal. For a more precise analysis of the roughness statistics of the lipid film, it would be useful to study the diffuse scattering as described in refs 54 and 58.

The lines in Figures 4 and 5 depict the theoretical curves. These lines were obtained both with the model-based approach (green lines, dashed is for $\sigma_0 \equiv 0$, in Figure 5) with the interfacial structure represented by the two layers and with the model-independent approach (blue lines), where no assumption about the structure was required. The red lines show the results of the direct MD calculations for the studied systems.

MD Simulations. DMPS monolayers are so well suited for computational methods that the electron density profiles can be used to validate the MD simulations. Their successive comparison allows us to analyze changes in the molecular structure and the variation in the boundary potential occurring during the compression of the monolayer.

To associate the electron density profile with the molecular structure of the lipid monolayer, we performed MD simulations for systems with the following areas per lipid: 37, 41, 45, 50, 61, 70, 80, 91, and 181 Å^2 (see Figure 1). Although a monolayer with area per lipid <40 Å^2 is impossible to prepare experimentally, it can still be modeled using molecular dynamics. Red lines in Figures 4 and 5 show the reflectivity curves and electron density profile reconstructed from the MD simulations. These curves were compared to the X-ray reflectivity data and the data calculated with the model-based and model-independent approaches. All the curves correlate quite well at various areas per molecule in the monolayer. This result reliably validates our MD simulations and allows us to highlight fine details of the interfacial structure with the following simulations.

For samples with $A = 41$ Å^2 and $A = A_C$, the reflectivity curves do not demonstrate a significant difference between each other and they are described by the same MD simulation with $A = 41$ Å^2 (Figures 4e,f and 5e,f). Thus, the monolayer reaches the highest density at $A_C \approx 40$ Å^2 that is in agreement with the grazing incidence diffraction data (∼20 Å^2 per acyl chain) near the collapse.[25,59]

Visualizing the equilibrium trajectory parts, we observe a regular monolayer in simulated systems for the following area per lipid values: 37, 41, 45, 50, 61, 70, and 80 Å^2. In the state of 41 Å^2, we noticed some signs of collapse. In the system with $A =$ 37 Å^2, the area per lipid is less than A_C, so that the monolayer is over compressed and small out of plane undulations are observed in its simulated structure. At the same time, highly diluted monolayers (at 90 Å^2 and more) exhibit some lipid segregation at the interface. Snapshots (front and side views) for several monolayer dilutions are presented in Figure S3. These snapshots illustrate the transformation of the monolayer from a segregated state to a continuous state. Note that this transformation is not reflected in the shape of the pressure and potential diagrams (Figure 1). In the cases of a continuous monolayer, the MD data show differences in the lateral organization of the lipids (Figure S2). Almost completely unordered lateral packing is observed at 60 Å^2, which then becomes highly ordered hexagonal packing at 45 Å^2. The molecular nature of these phenomena is clarified by the presentation of the distribution of different components of the system normal to the monolayer (see Figure 6).

The interfacial structure simulated by MD allows us to visualize the individual contributions of the lipid head groups, hydrophobic acyl chains, and the associated water molecules to the electron density. Looking at the hydrophobic tail density (solid gray curves in Figure 6), we observe a considerable transformation from a smooth Gaussian profile in the diluted noncontinuous monolayers ("a" and "b") to graded profiles in the highly packed monolayers ("e" and "f"). This transformation is reflected in the total electron density profiles as the distinct shoulder in the corresponding curves. It seems that the hydrocarbon tails are responsible for a plateau at distances between −25 and −17 Å in panels "e" and "f" that correspond to the monolayers in the condensed LC phase. Thus, a continuous and relatively uniform layer looks like an "alkane liquid" formed by hydrocarbon tails. In contrast, in the diluted monolayers, the hydrocarbon tail input to the electron density increases smoothly until the water density becomes essential (compare the gray curves in panels "a", "b", and "c"). The mentioned difference between the hydrocarbon chain input can be

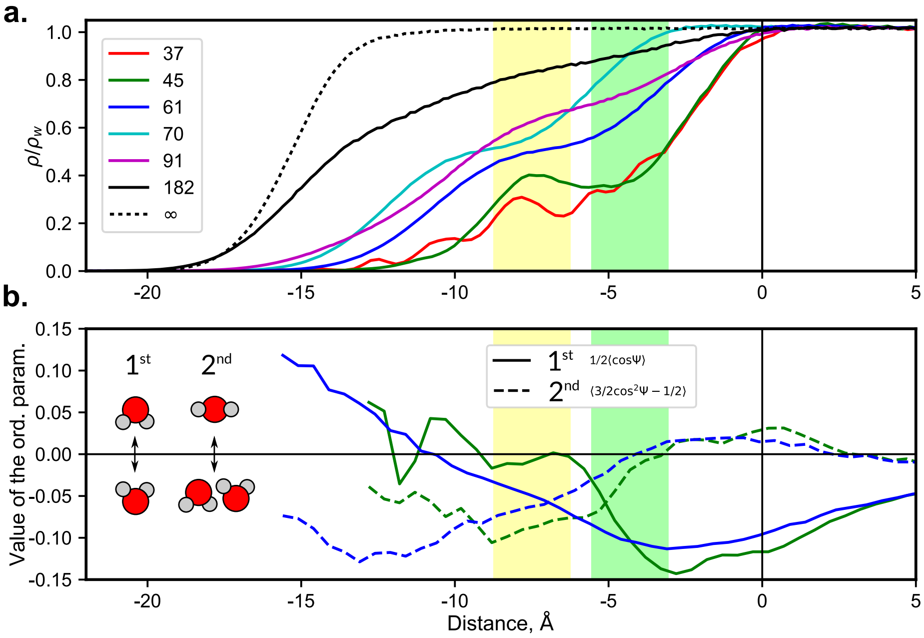

Figure 7. (a) Electron density profile of the water molecules for a series of monolayers with different surface densities of the lipids. The numbers for the colored curves correspond to the area per lipid (Å^2) in the monolayers, with an infinity sign for the pure water−air interface. (b) Depicts the 1st (solid lines) and 2nd (dashed lines) orientation order parameters plotted for the monolayers in the LE state (61 Å^2, blue) and in the LC state (45 Å^2, green). The cartoon with the water molecules on the left side illustrates their orientation for positive and negative values of the order parameters. The zero at the abscissa axis corresponds to the boundary between the outer plane of the head group block and the water surface.

attributed to the variation in the angle between the average tail direction and the monolayer surface, which is large for diluted monolayers. The shape of the curves for the lipid head groups (Figure 6, red lines) varies with the lipid surface density, but this result is not reflected in the integral electron density in the range of −15−0 Å. This occurs because lipid head groups are immersed into the water bulk as long as the monolayer is diluted. The head group immersion follows from the water profile near the point of −10 Å in different panels of Figure 6. The potassium cations contribute to the electron density of the head group region along with phosphate groups (Figure 6, yellow curves), although this contribution is insignificant.

The numerical details of the monolayer structure and the estimates of the parameters of the two-layer model (eq A1) are presented in Table 1. On one hand, the thickness of head group region, L_1, weakly depends on the state of the monolayer. On the other hand, its density, ρ_1, increases markedly with the decreasing area, A, because of the accumulation of the dense lipid head groups in the region of the hydrophilic slab. Both the two-layer model and the MD data demonstrate that the thickness of the hydrophobic tail region L_2 increases with decreasing area, A. This is due to the decrease of the tilt angle of the acyl chains upon the compression of the monolayer. The contribution of the chains to the electron density doubles and remains constant in the LC state. Our results are in good agreement with an earlier report by Helm et al. on the structure of DLPE−DMPE monolayers, in which the authors also registered an increase in the density of the head group region during compression, accompanied by a thickening of the hydrophobic slab.[60]

According to our MD analysis, the average number of H_2O molecules, n^*, which is associated with the polar groups of lipids, decreases with the transition from the diluted ($n^* \approx 75$) to the condensed state of the monolayer ($n^* \approx 6$). We also evaluated the hydration number, n, from the two-layer model (see Appendix I). In Table 1, the data sets for n and n^* are in qualitative agreement. Both n and n^* are sensitive to the position of the lipid−water interface. Therefore, we do not expect the quantitative agreement between the hydration numbers calculated from such different approaches. Moreover, the difference in absolute values can be explained by both the low spatial resolution of the X-ray data and the insufficiency of the two-layer model. In particular, n^* is greater than n at $A < 60$ Å^2, due to the simplified consideration of potassium adsorption used in the analysis of X-ray data, provided that only one cation is attached to the lipid, which is usually incorrect.

Water extrusion from the interface by lipid molecules is illustrated in detail in Figure 7. This effect is rather complicated since the water fraction expelled from the monolayer changes with its compression. The water profile for the 45 Å^2 monolayer (Figure 7a, green curve) exhibits a clear peak at a distance between −9 and −7 Å. This fraction of water is noticeable for almost every lipid density and is visible at the density plot as the distinct shoulder at 61 Å^2 (blue curve), as the small perturbation at 91 Å^2 (magenta curve), and as the small visible peak at 37 Å^2 (red curve). This layer of water is very thin and consists of specially oriented molecules. Water molecules are embedded in the coordination envelope of head groups since this layer is located close to the peak of the phosphate group (Figure 6, yellow). Note that another peak of the same fraction is visible at 45 Å^2 and is significantly smoothed when the monolayer is diluted up to 61 Å^2 per lipid.

It is interesting to note the water dipole orientation in the compact and diluted states by calculating the so-called order parameters (Figure 7b). These parameters are equal to zero when water is disoriented. The first-order parameter is positive when the dipole of water is oriented toward the bulk, is negative for the orientation toward the air, and is zero when it is parallel to the surface. On the contrary, the second-order parameter is negative if the dipole of H_2O is parallel to the plane of the monolayer and positive when perpendicular to the plane. Order parameter profiles are in good agreement with those recently calculated for DPPC, with the exception of minor deviations.[61] In the LC state, the dipole orientation in a narrow region in the vicinity of −8 Å (Figure 7, left yellow zone) is characterized by a large absolute value of the second-order parameter (Figure 7b, green dashed line). However, these molecules have an average zero dipole projection in the normal direction, which corresponds to a low absolute value of the first-order parameter (Figure 7b, solid green line). After melting, in the liquid state (blue curves), the first-order parameter at approximately −8 Å is negative and the second-order parameter slightly shifts to zero. Thus, we may conclude that this thin layer corresponds to tightly bound water molecules and that their orientation becomes sensitive to the phase state. Another significant portion of water, which is intensively extruded during the LE−LC phase transition, is situated in the layer between −3 and −6 Å (Figure 7, right green zone). The value of the first-order parameter in it is so negative that dipoles of H_2O are strongly orientated toward the air. Their extrusion from this layer naturally leads to a decrease of the oriented water's contribution to the Volta potential.

Several of our results of the present paper are in good agreement with the data in the literature known for other lipid systems and related to the general properties of amphiphilic systems.

1. Discontinuous monolayer formation commencing at 90 $Å^2$ per molecule is a general phenomenon that results from the ability of amphiphilic molecules to aggregate at the interface. This was demonstrated by mixed monolayer simulations for a DPPC−POPC system with a Slipids force field.[62]
2. Upon monolayer compression, hexagonally ordered subphases are expected for any lipids that have a phase coexistence region in their pressure−area isotherms (e.g., DMPS and DPPC). This effect was described for the DPPC monolayer in both coarse grain simulations[29] and all-atom simulations.[20,22]
3. The reduction in the tail layer thickness upon monolayer dilution may not depend on the nature of the lipid. Indeed, this was demonstrated in spectroscopic studies of the DPPC monolayer[3] and in MD simulations of the same monolayer.[20]
4. The head group immersion into the bulk in diluted monolayers was first observed in an MD study of DPPC monolayers (see Figure 8 in ref 19). However, the authors did not discuss this result, and no experimental data were used to confirm it.

The two peaks in Figure 6 for the hydrophobic tails and head groups (gray and solid red lines) are placed separately at every lipid density. This feature is consistent with the model-based approach with a two-layer structure of the interface used previously in X-ray data analysis (eq A1). The width of the tail layer in the condensed monolayers is nearly the same as the length of the myristoyl tail in the DMPS chemical structure (Figure 2, right). The two layers (or slabs in terms of the model) are represented by the red dashed lines in Figure 6. The area under the curves in this figure is related to the amount of material. The area of the first block is roughly equal to the area under the curve of the hydrocarbon tail density (gray lines). Thus, the first block in the model-based approach directly corresponds to the hydrocarbon tails. As pointed out before, the head group region of the electron density cannot be interpreted in the same simple way. The proper block reflects the number of head groups in the interface for dense monolayers only. A diluted monolayer includes a large number of water molecules in the head group layer. These molecules are associated with the head groups and strongly oriented according to a series of recent simulations in a similar environment.[17,30,46,61] It seems evident that extremely oriented water molecules could hardly be removed from the lipid head groups because they are strongly H-bonded with the phosphate and carbonyl oxygen atoms.

According to our MD data, the decomposition of the electron density corresponds well to the data of several papers based on MD simulations of different monolayers. It was concluded[30,63] that the maximal electron density value corresponds to the peak of the phosphate group, positioned at the same place as in Figure 6 (yellow curves). Relative to the bulk of water, this position agrees with the X-ray reflectivity data analysis suggested in ref 63 for the DMPA and DPPC monolayers.

Electric Potentials at the Interface. In the previous sections, we focused on the water extrusion from the polar head group region caused by the compression of the lipid monolayer. Here, we focus our attention to the water fraction, which contributes significantly to the electric potential at the interface. The Volta potential of the lipid monolayer measured in a real experiment (Figure 1, red) is the difference between two water−air Galvani potentials registered in the presence and absence of a lipid monolayer.[64] Note that a compression of charged molecules has some effects on the potential drop over the electrical double layer close to the interface and decreases the amplitude of the Volta potential. The magnitude of this effect depends on both the screening of the surface and the adsorption of inorganic cations. The variation in the Volta potential with the change in the surface density of charged lipids can be estimated in the framework of the Gouy−Chapman theory.[65−67] At an ionic strength as high as 100 mM KCl, it is in the range from 30 to 50 mV. Thus, the variations in the boundary Volta potential, both found in the experiment and obtained from the simulations, are mainly associated with the dipole reorientation in the lipid monolayer during its compression. The same is true for the Volta potential amplitude in MD simulations. The total electric potential was calculated from the charge density for every simulated monolayer; the results are presented in Figure S1. The absolute values of the Volta potential are comparable to the experimental data when the optical dielectric permittivity of water ($n^2 = 1.77$) is used for the calculation. These values of the Volta potential are compared with the experimental data in Figure 8. Again, the abscissa in the figure is transformed hyperbolically to reveal the linear dependence of the potential on the inverted density. In this case, there is a visible correspondence between the Volta potential in the LE state (60−80 $Å^2$) and the Helmholtz equation:[64]

$$\Delta V = 12\pi\mu \times \Delta(A^{-1}) \tag{3}$$

where the potential is measured in mV, the area per lipid A is measured in $Å^2$, and the dipole moment, μ, is measured in milliDebye units (mD).

The experimental curve of the potential has a visible singularity in the phase coexistence region (Figure 8). According to the experimental data and eq 3, the transition from the LE phase to the LC phase leads to an increase in the dipole moment from 500 to 570 mD. At the highest lateral pressure, the Volta potential achieves its maximal value in the plateau. All of the trends mentioned in the experiment are reproduced by the MD

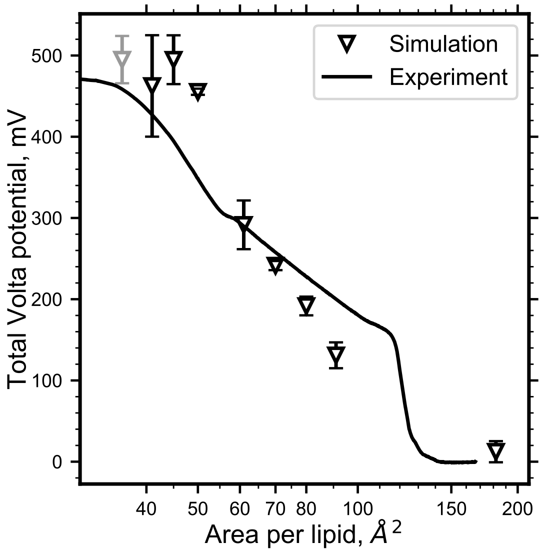

Figure 8. Compression diagram of the Volta potential (solid) and summary boundary potential of the monolayer obtained from the simulation (triangles) calculated by eq 3. The abscissa is transformed hyperbolically (see the legend of Figure 1 and the comments in the text).

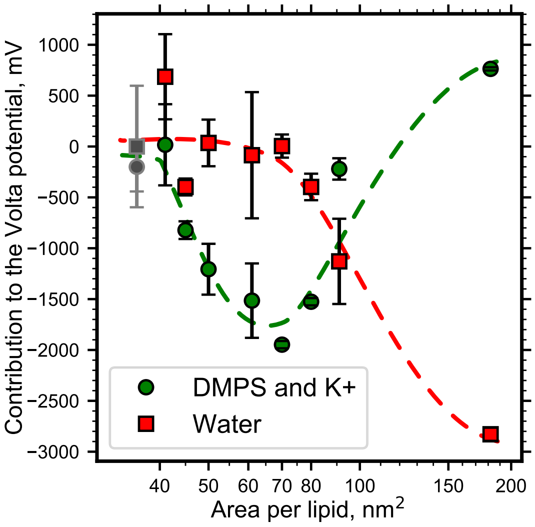

Figure 9. Relative changes in the contributions of the "lipid + counterion" subsystem (green circles) and the water molecules subsystem (red squares) to the total boundary potential of the DMPS monolayer at several values of the area per molecule.

modeling with the calculated Volta potential values, which are comparable to the experimental values (Figure 8, triangular points). Note that the direct simulation of the Volta potential is problematic due to the lack of its full thermodynamic description.[68]

MD modeling can reveal the molecular nature of some interesting electrostatic effects related to the interface structure: the change in the integral dipole moment, its singularity in the phase transition, and the saturation of the Volta potential at high lipid densities. The water extrusion during the LE−LC phase transition should critically contribute to the change in the Volta (boundary) potential. First, we return to the shape of the water density profile in the systems at 45 and 61 Å^2 (Figure 7). When the monolayer became more compact in the phase transition, the water molecules extruded mostly from the layer between distances of −7 and −2 Å (Figure 7a). Previously, we pointed out that the thin layer at approximately −8 Å consisted of water molecules tightly fixed to the head groups. In contrast, the first-order parameter is negative, while the second-order parameter is approximately zero for molecules placed in the layer between −7 and −2 Å. Since these molecules are mobile, they are the main contributors to the change in the electric potential during the transition.

Next, we analyze the contribution of the water molecules and the other components of the system to the boundary potential separately. Their inputs have large absolute values (up to several volts) but the opposite signs: positive for the water subsystem and negative for the lipid−counterion part. Their sum makes the total potential less than 1 V as measured in the experiment. Previously, several authors discussed the positive sign of the contribution of the water subsystem to the boundary potential of a phospholipid monolayer.[64,69,70] In Figure 9, we demonstrate the relative contributions of both subsystems to the potential under various states of compression. During compression, the potential grows as the water input increases until the area per lipid reaches 70 Å^2. In the most compact state, the water input is constant, and the lipid−counterion subsystem is responsible for the change in the potential. We may suppose that the water subsystem does not provide any input to the potential in this case, since water molecules are extruded in the phase transition from the LE state to the LC state (see above). At the same time, as the lipid subsystem becomes ordered upon compression, the hydrophobic tails also become oriented at the interface so that the dipoles at the ends of the methyl groups provide a substantial input to the potential. Such behavior is represented in the potential profiles (Figure S1) as a narrow peak at a depth from −30 to −20 Å. The physical causes of the origin of the surface dipole moment are considered in detail by Brockman (see equations 2 and 3 in ref 64). Naturally, the scale of the related effects depends on the force field used in the MD simulations (OPLS/Amber/CHARMM), since small changes in the C and H atomic charge at the edge CH_3 groups decidedly influence the dipole potential. Note that a similar approach to study the nature of the dipole potential was performed by MD simulations of DPPC monolayers.[22] The authors decomposed the potential into two subsystems and compared the inputs at different monolayer densities. They identified a similar behavior between water and lipid inputs under monolayer compression in the noticeably smaller A range from 40 to 70 Å^2. However, the validity of these conclusions is questionable, because the production trajectories of the simulations were too short (10 ns). Note that, in the case of fluorinated acyl chains, the dipole moment of the $-CF_3$ group has a direction opposite to that of the $-CH_3$ group. Therefore, it is expected that the Volta potential should decrease with compression. Indeed, this effect was observed in an experiment with fluorinated DPPC.[71]

■ CONCLUSIONS

For the first time, we carried out a detailed comparison of X-ray reflectivity experimental data and MD simulated data over a wide range of the monolayer compression stages. The study was motivated by several facts mentioned in the preface concerning the biological significance of electrostatic phenomena at the surface of cell membranes accompanied by condensation of the negatively charged membrane component: PS. In particular, interest was paid both to the phase state of the membranes and to the Langmuir technique, which was applied as a tool, to study

DOI: 10.1021/acs.langmuir.9b01450
Langmuir 2019, 35, 12326−12338

the most adequate model system: monolayers of the dimyristoyl derivative of PS. The MD simulations and advanced data analysis of the X-ray reflectivity data for the same monolayer systems allowed us to identify new details of the structure at the lipid−water interface and then associate these details with the electrical properties of this interface.

For any compression state of the DMPS monolayer in the range from 40 to 200 Å^2 per lipid, the comparison between the electron density profile reconstructed from the X-ray data and the data obtained directly from the MD simulations demonstrates excellent agreement between them. To resolve the inverse problem of X-ray reflectivity at a sufficiently high credibility level to obtain information about the surface-normal interfacial structure, we used two completely independent approaches. The first approach uses some a priori information about polar and hydrophobic layers at the interface (the "model" approach), and the second approach makes no assumptions about the interface structure ("model-less" approach). The former approach is useful for a direct comparison with MD data in terms of molecular structure. The latter approach shows a great ability to rebuild the absolute values of electron density from X-ray experimental data without a priori assumptions about the interfacial structure. Since both approaches result in almost identical profiles, our conclusions regarding the structure of the monolayers are rather unambiguous and sufficiently credible. To compare the MD simulations with the recovered electron density profiles, we found that it was mandatory to smooth the former profiles due to the distortion originating from thermally activated capillary waves. According to this analysis, for example, for the strongest compression states, the water displaced from the polar region. The increment of the hydrophobic tail region under compression follows from both the X-ray and simulation data and is presumably caused by the ordering of acyl chains along one direction.

Finally, using the compression scenario, we explain the behavior of the Volta potential. On one hand, the potential is described by the Helmholtz equation in both the LE state and the "cluster" state. In these states, the Volta potential is defined by the surface concentration of elementary dipoles associated with lipid molecules enriched with the oriented water molecules. On the other hand, upon compression, the oriented water extruded from lipid polar groups and the values of the elementary dipoles increase due to a preferred orientation of acyl chains $-C_{13}H_{27}$ so that the Volta potential saturates and approaches the plateau when the monolayer is close to collapsing. We were able to obtain details on the evolution of the interfacial structure upon compression of the DMPS monolayer only by combining two independent approaches for X-ray reflectivity data analysis with the comparison of the results with the MD simulated data. We suggest that the basic details of both the phase transition and the electric potentials discussed for the DMPS monolayers describe a common picture for other lipid structures as well.

■ APPENDIX I

In the model-based approach, the reflectivity data were analyzed by a two-slab model, where one slab represents the average electron density in the head group region of the lipids and the other slab represents the electron density in the acyl group region. Thus, the postulated model for the surface-normal electron density profile is given by

$$\rho(z) = \frac{1}{2}\rho_0 + \frac{1}{2}\sum_{j=0}^{2}(\rho_{j+1} - \rho_j)\,\mathrm{erf}\left(\frac{l_j}{\sigma_0\sqrt{2}}\right),$$
$$l_j(z) = z - \sum_{n=0}^{j} L_n, \qquad \mathrm{erf}(x) = \frac{2}{\sqrt{\pi}}\int_0^x \mathrm{e}^{-y^2}\,\mathrm{d}y \tag{A1}$$

where $\rho_0 \equiv \rho_w$ is the electron density in the water's bulk ($\rho_w \approx$ 0.333 e$^-$/Å^3), $L_0 \equiv 0$ is the position of the water−polar group interface ($z = 0$), and $\rho_3 = 0$ is the electron density in the air. L_1 and L_2 are the thicknesses of the head group and acyl group regions, respectively; ρ_1 and ρ_2 represent the average electron densities of the head group and acyl group regions, respectively, and σ_0 is the roughness of the surface determined primarily by capillary waves.[55] The first term in the sum in eq A1 represents the interface between the bottom of the head group region and the water substrate; the second term represents the interface between the bottom of the acyl group region and the head group region, and the third term represents the interface between the vapor and the top of the lipid acyl group. Corresponding to eq A1, the X-ray reflectivity is given by the following:

$$R(q_z) \approx \frac{\exp(-\sigma_0{}^2 q_z q_z^t)}{\rho_w{}^2}\left|\frac{q_z - q_z^t}{q_z + q_z^t}\right|^2$$
$$\left|\sum_{j=0}^{2}(\rho_{j+1} - \rho_j)\exp\left(i\sqrt{q_z q_z^t}\,\textstyle\sum_{n=0}^{j} L_n\right)\right|^2 \tag{A2}$$

where $q_z' = \sqrt{q_z{}^2 - q_c{}^2}$ and $q_c = 2k_0 \sin \alpha_c \approx 0.022$ Å^{-1}.

In our calculations, the parameter σ_0 is specified by the short wavelength limit in the spectrum of capillary waves $Q_{max} = 2\pi/a$ ($a \approx 10$ Å is the order of magnitude of the intermolecular distance) and the angular resolution of the detector, $Q_{min} = q_z^{max}\Delta\beta$ so that

$$\sigma_0{}^2 = \frac{k_B T}{2\pi\gamma(A)}\ln\left[\frac{Q_{max}}{Q_{min}}\right] \tag{A3}$$

where k_B is the Boltzmann constant.[34,72,73] $\gamma(A)$ is the surface tension that also defines the surface pressure diagram $\Pi(A) = \gamma_0 - \gamma(A)$, where $\gamma_0 \approx 72$ mN/m under normal conditions.

The reflectivity calculated from eq A2 is then fit to the data to yield values for the following fitting parameters: ρ_1, ρ_2, L_1, L_2, and σ_0. Note that, if σ_0 is given as one of the optimization parameters, its value, σ_{fit}, is found to be in the range from 2.6 to ∼4 Å, which corresponds roughly to the range of the values calculated using eq A3 (see Table 1). The errors of the determination of the parameters were evaluated by the standard χ^2 criterion at a confidence level of ∼0.9.

The second approach with no a priori assumption regarding the structure of the sample is based on the extrapolation of the asymptotic behavior of the reflectivity curve to the range of $q_z \to \infty$.[53,54] In this model-independent approach, the only postulation used is that the polarizability distribution $\delta(z)$ contains a number of "discontinuity points" at which either the function $\delta(z)$ itself or its n-th derivative exhibits a step-like variation $\Delta^n(z_j) = d^n\delta(z_j + 0)/dz^n\delta - d^n\delta(z_j - 0)/dz^n$, where z_j is the coordinate of the j-th discontinuity point.

A combination of such points unambiguously defines the asymptotic behavior of amplitude reflectivity factor $r(q_z)$ at $q_z \to \infty$

$$r_{as}(q_z \to \infty) - \left(\frac{2\pi}{\lambda}\right)^2 \left(\frac{i}{q_z}\right)^{n+2} \sum_{j=1}^{m} \Delta^{(n)}(z_j)e^{iq_z z_j} \qquad \text{(A4)}$$

As shown in ref 53, in the general case, there are only two physically reasonable distributions of $\delta(z)$, which correspond to both experimental and absolute values of the reflectivity $R(q_z) = |r(q_z)|^2$ measured within a limited range of q_z and given a combination of m discontinuity points $\Delta^{(n)}(z_j)$ defining the asymptotic $r_{as}(q_z \to \infty)$.

Hence, in the model-independent reconstruction of the polarizability distribution, one must find the order and locations of the discontinuity points for the target structure. In the present paper, we used a modified Fourier transform of the experimental reflectivity curves.[54] For all of our reflectivity data, at least one discontinuity point of the first order was found that corresponds to asymptotic behavior $R(q_z) \propto 1/q_z^6$.

The target polarizability profile $\delta(z)$ has been represented by the stepwise distribution $\delta(z_1, ..., z_M) = \sum_{m=1}^{M} \Delta^n(z_m)H(z - z_m)$ where $H(z)$ is the Heaviside function, with a number of steps of $M \sim 100$ and fixed locations of the discontinuity points $\Delta^1(z_j)$ The reflectivity factor $R_c(q_z, \delta(z_1)...\delta(Z_M))$ has been calculated using Parratt's recurrent formulas.[74] Then, the calculated reflectivity curve was fitted to the experimental data $R(q_z)$ by the standard Levenberg−Marquardt algorithm to find the optimal profile $\delta(z_1...z_M)$ as free-form fitting parameters. All calculations were implemented in the Python language with the use of the numpy/scipy libraries.

Note that the quality of the discussed experimental X-ray data is sufficiently high to reliably establish the extrusion of the oriented water molecules from the lipid polar groups. For the LE state, the thickness of $L \approx 20$ Å and the distance between the singular points in the profile $\rho(z)$ of the model-less approach, approximately 16 Å, are appreciably smaller than the length of the lipid molecule, approximately 27 Å (Table 1). This suggests that the hydrocarbon chains of the molecules in the liquid phase of the lipid ($A > 60$ Å^2) are disordered relative to the surface normal.

For the LC state ($A \approx 40$ Å^2), the thickness of the second layer of $L_2 \approx 15$ Å roughly (Table 1) corresponds to the calculated length of the hydrocarbon tails $-C_{13}H_{27}$ in the DMPS molecule, 16.7 Å (≈12× 1.27 Å (C−C) + 1.5 Å ($-CH_3$)). The density $\rho_2 \approx 0.95\rho_w$ and the area per hydrocarbon chain $A/2 \approx 18$ Å^2 correspond to one of the ordered phases of the long-chain saturated hydrocarbons.[75] Thus, the deflection angle of the molecular tail axis from the surface normal can be estimated to be as much as arccos(15/16.7) ≈ 26° (26° ± 6°).

Note that the imbalance in the number of electrons per structural unit is observed for all states. For example, in the LC state, the numbers of electrons accounted by the polar part of the DMPS molecule and the aliphatic tails are $\rho_1 AL_1 \approx 220$ e$^-$ and $\rho_2 AL_2 \approx 190$ e$^-$, respectively. The excess electron density, $\delta\Gamma$, in the layer of the heads is $\delta\Gamma = A(\rho_1 L_1 - \rho_2 L_2 \Gamma_h/\Gamma_t) \approx 80$ e$^-$ per DMPS molecule, which is equivalent to $\delta\Gamma/\Gamma_w \approx 8$ H_2O molecules ($\Gamma_w = 10$ is the number of electrons in H_2O). The total number of electrons in potassium salt $C_{34}H_{65}NO_{10}PK^+$ is $\Gamma_h + \Gamma_t = 390$, where $\Gamma_h = 180$ and $\Gamma_t/2 = 105$ are the numbers of electrons in the PS group with K$^+$ and the hydrocarbon tail $-C_{13}H_{27}$, respectively. Such a degree of hydration was reported previously for the gel phase of phospholipids by Mohwald.[1] If the electron density is taken as a rough estimate of the degree of hydration, then it increases more than 2-fold as the area per molecule increases from $A \approx 40$ Å^2 to $A \approx 91$ Å^2, where for the latter case there are ~30 H_2O molecules per polar group. Alternatively, the average number of water molecules, n, per lipid molecule (see Table 1) can be estimated using the following equation: $n = (1/\Gamma_w)(A\rho_1 L_1 + A\rho_2 L_2 - \Gamma_h - \Gamma_t)$. For LC phase, $n \approx 3$ when $\delta\Gamma/\Gamma_w \approx 8$. On the one hand, the difference in hydration numbers demonstrated by these two approaches shows that the two-layer model under discussion does not unambiguously describe the interfacial atomic structure. On the other hand, its use is determined by the rather low spatial resolution of the presented X-ray data so that more complex models also cannot eliminate this ambiguity.

■ ASSOCIATED CONTENT

Ⓢ Supporting Information

The Supporting Information is available free of charge on the ACS Publications website at DOI: 10.1021/acs.langmuir.9b01450.

Video where all the Delaunay triangles are visible (unlike in Figure S2), constructed by averaging the simulation over a time interval of 1 ns (MPG)

Video where all the Delaunay triangles are visible (unlike in Figure S2), constructed by averaging the simulation over a time interval of 1 ns(MPG)

Video where all the Delaunay triangles are visible (unlike in Figure S2), constructed by averaging the simulation over a time interval of 1 ns (MPG)

Details on the MD simulated monolayer systems (Table S1, Figures S1−S3) (PDF)

■ AUTHOR INFORMATION

Corresponding Authors

*E-mail: yury.a.ermakov@gmail.com.
*E-mail: comcon1@protonmail.com.
*E-mail: tikhonov@kapitza.ras.ru.

ORCID

A. M. Tikhonov: 0000-0003-2013-1158

Notes

The authors declare no competing financial interest.

■ ACKNOWLEDGMENTS

The authors thank the Sector of Biophysics and Computer Science of Complex Systems at the Department of Biophysics (MSU, Biological faculty). This work was supported by the Ministry of Science and Higher Education within the State assignments for the institutes of RAS. The authors acknowledge Russian Science Foundation for funding the X-ray measurements (Project No. 15-12-00030) and X-ray reflectivity analysis (Project No. 18-12-00108). The work of Y.A.E. was supported by Grant #19-04-00242a from the Russian Foundation for Basic Research. The work of A.M.N. was supported by a Russian President Scholarship (SP-511.2018.4).

■ REFERENCES

(1) Mohwald, H. Phospholipid monolayers. In *Handbook of Biological Physics*; Lipowsky, R., Sackmann, E., Eds.; Elsevier Science B.V.: 1995; pp 161−211.

(2) Stefaniu, C.; Brezesinski, G.; Mohwald, H. Langmuir monolayers as models to study processes at membrane surfaces. *Adv. Colloid Interface Sci.* **2014**, *208*, 197−213.

(3) Ma, G.; Allen, H. C. DPPC Langmuir Monolayer at the Air-Water Interface: Probing the Tail and Head Groups by Vibrational Sum Frequency Generation Spectroscopy. *Langmuir* **2006**, *22*, 5341−5349.

(4) McConlogue, C. W.; Vanderlick, T. K. A Close Look at Domain Formation in DPPC Monolayers. *Langmuir* **1997**, *13*, 7158−7164.

(5) Okulski, W.; Sujak, A.; Gruszecki, W. I. Dipalmitoylphosphatidylcholine membranes modified with zeaxanthin: numeric study of membrane organisation. *Biochim. Biophys. Acta, Biomembr.* **2000**, *1509* (1−2), 216−228.

(6) Toimil, P.; Prieto, G.; Minones, J., Jr.; Sarmiento, F. A comparative study of F-DPPC/DPPC mixed monolayers. Influence of subphase temperature on F-DPPC and DPPC monolayers. *Phys. Chem. Chem. Phys.* **2010**, *12* (40), 13323−13332.

(7) Andelman, D.; Brochard, F.; Joanny, J.-F. Phase transitions in Langmuir monolayers of polar molecules. *J. Chem. Phys.* **1987**, *86* (6), 3673−3681.

(8) Shushkov, Ph; Tzvetanov, S.; Velinova, M.; Ivanova, A.; Tadjer, A. Structural Aspects of Lipid Monolayers: Computer Simulation Analyses. *Langmuir* **2010**, *26* (11), 8081−8092.

(9) Mohwald, H. The phases and phase transitions of lipid monolayers. *Phase Transitions in Soft Condensed Matter* **1989**, *211*, 145−159.

(10) Pfeiffer, H.; Binder, H.; Klose, G.; Heremans, K. Hydration pressure and phase transitions of phospholipids I. Piezotropic approach. *Biochim. Biophys. Acta, Biomembr.* **2003**, *1609*, 144−147.

(11) Pfeiffer, H.; Binder, H.; Klose, G.; Heremans, K. Hydration pressure and phase transitions of phospholipids II. Thermotropic approach. *Biochim. Biophys. Acta, Biomembr.* **2003**, *1609*, 148−152.

(12) Ruckenstein, E.; Li, B. Q. A simple surface equation of state for the phase transition in phospholipid monolayers. *Langmuir* **1996**, *12* (9), 2308−2315.

(13) McConnell, H. M. Structures and transitions in lipid monolayers at the air-water interface. *Annu. Rev. Phys. Chem.* **1991**, *42*, 171−195.

(14) Knobler, C. M.; Desai, R. C. Phase transitions in monolayers. *Annu. Rev. Phys. Chem.* **1992**, *43*, 207−236.

(15) Ermakov, Y. A.; Averbakh, A. Z.; Yusipovich, A. I.; Sukharev, S. Dipole potentials indicate restructuring of the membrane interface induced by gadolinium and beryllium ions. *Biophys. J.* **2001**, *80* (4), 1851−1862.

(16) Ermakov, Y. A.; Kamaraju, K.; Sengupta, K.; Sukharev, S. Gadolinium ions block mechanosensitive channels by altering the packing and lateral pressure of anionic lipids. *Biophys. J.* **2010**, *98* (6), 1018−1027.

(17) Feller, S. E.; Zhang, Y.; Pastor, R. W. Computer simulation of liquid/liquid interfaces. II. Surface tension-area dependence of a bilayer and monolayer. *J. Chem. Phys.* **1995**, *103* (23), 10267−10276.

(18) Mauk, A. W.; Chaikof, E. L.; Ludovice, P. J. Structural Characterization of Self-Assembled Lipid Monolayers by *NpT* Simulation. *Langmuir* **1998**, *14*, 5255−5266.

(19) Lopez Cascales, J. J.; Otero, T. F.; Fernandez Romero, A. J.; Camacho, L. Phase transition of a DPPC bilayer induced by an external surface pressure: from bilayer to monolayer behavior. a molecular dynamics simulation study. *Langmuir* **2006**, *22* (13), 5818−5824.

(20) Mohammad-Aghaie, D.; Mace, E.; Sennoga, C. A.; Seddon, J. M.; Bresme, F. Molecular dynamics simulations of liquid condensed to liquid expanded transitions in DPPC monolayers. *J. Phys. Chem. B* **2010**, *114* (3), 1325−1335.

(21) Baoukina, S.; Monticelli, L.; Marrink, S.-J.; Tieleman, D. P. Pressure-Area Isotherm of a Lipid Monolayer from Molecular Dynamics Simulations. *Langmuir* **2007**, *23*, 12617−12623.

(22) Tzvetanov, S.; Shushkov, P.; Velinova, M.; Ivanova, A.; Tadjer, A. Molecular dynamics study of the electric and dielectric properties of model DPPC and dicaprin insoluble monolayers: size effect. *Langmuir* **2010**, *26* (11), 8093−8105.

(23) Kaznessis, Y. N.; Kim, S.; Larson, R. G. Simulations of zwitterionic and anionic phospholipid monolayers. *Biophys. J.* **2002**, *82* (4), 1731−1742.

(24) Kago, K.; Matsuoka, H.; Yoshitome, R.; Yamaoka, H.; Ijiro, K.; Shimomura, M. Direct in Situ Observation of a Lipid Monolayer-DNA Complex at the Air-Water Interface by X-ray Reflectometry. *Langmuir* **1999**, *15*, 5193−5196.

(25) Kaganer, V. M.; Mohwald, H.; Dutta, P. Structure and phase transitions in Langmuir monolayers. *Rev. Mod. Phys.* **1999**, *71* (3), 779−819.

(26) Bitto, E.; Li, M.; Tikhonov, A. M.; Schlossman, M. L.; Cho, W. Mechanism of annexin I-mediated membrane aggregation. *Biochemistry* **2000**, *39* (44), 13469−13477.

(27) Kucerka, N.; Gallova, J.; Uhrikova, D.; Balgavy, P.; Katsaras, J. The need to revisit lipid areas. *Journal of Physics: Conference Series* **2010**, *251* (1), 012043.

(28) Duncan, S. L.; Dalal, I. S.; Larson, R. G. Molecular dynamics simulation of phase transitions in model lung surfactant monolayers. *Biochim. Biophys. Acta, Biomembr.* **2011**, *1808* (10), 2450−2465.

(29) Baoukina, S.; Monticelli, L.; Marrink, S.-J.; Tieleman, D. P. Pressure-Area Isotherm of a Lipid Monolayer from Molecular Dynamics Simulations. *Langmuir* **2007**, *23*, 12617−12623.

(30) Helm, C. A.; Mohwald, H.; Kjaer, K.; Als-Nielsen, J. Phospholipid Monolayer Density Distribution Perpendicular to the Water Surface. A Synchrotron X-Ray Reflectivity Study. *Europhys. Lett.* **1987**, *4* (6), 697−703.

(31) Schlossman, M. L.; Synal, D.; Guan, Y.; Meron, M.; Shea-McCarthy, G.; Huang, Z.; Acero, A.; Williams, S.; Rice, S. A.; Viccaro, P. J. A synchrotron x-ray liquid surface spectrometer. *Rev. Sci. Instrum.* **1997**, *68* (12), 4372−4384.

(32) Moehwald, H. PHOSPHOLIPID AND PHOSPHOLIPID-PROTEIN MONOLAYERS AT THE AIR-WATER INTERFACE. *Annu. Rev. Phys. Chem.* **1990**, *41*, 441−476.

(33) Lin, B.; Meron, M.; Gebhardt, J.; Graber, T.; Schlossman, M. L.; Viccaro, P. J. The liquid surface/interface spectrometer at ChemMatCARS synchrotron facility at the Advanced Photon Source. *Phys. B* **2003**, *B336*, 75−80.

(34) Braslau, A.; Deutsch, M.; Pershan, P. S.; Weiss, A. H.; Als-Nielsen, J.; Bohr, J. Surface Roughness of Water Measured by X-Ray Reflectivity. *Phys. Rev. Lett.* **1985**, *54* (2), 114−117.

(35) Danauskas, S. M.; Ratajczak, M. K.; Ishitsuka, Y.; Gebhardt, J.; Schultz, D.; Meron, M.; Lin, B.; Lee, K. Y. Monitoring x-ray beam damage on lipid films by an integrated Brewster angle microscope/x-ray diffractometer. *Rev. Sci. Instrum.* **2007**, *78* (10), 103705.

(36) Malkova, S.; Stahelin, R. V.; Pingali, S. V.; Cho, W.; Schlossman, M. L. Orientation and Penetration Depth of Monolayer-Bound p40phox-PX. *Biochemistry* **2006**, *45* (45), 13566−13575.

(37) Tietjen, G. T.; Baylon, J. L.; Kerr, D.; Gong, Z.; Henderson, J. M.; Heffern, C. T. R.; Meron, M.; Lin, B.; Schlossman, M. L.; Adams, E. J.; Tajkhorshid, E.; Lee, K. Y. C. Coupling X-Ray Reflectivity and In Silico Binding to Yield Dynamics of Membrane Recognition by Tim1. *Biophys. J.* **2017**, *113* (7), 1505−1519.

(38) Tikhonov, A. M.; Asadchikov, V. E.; Volkov, Yu. O.; Roshchin, B. S.; Ermakov, Yu. A. X-Ray Reflectometry of DMPS Monolayers on a Water Substrate. *J. Exp. Theor. Phys.* **2017**, *125* (6), 1051−1057.

(39) Asadchikov, V. E.; Volkov, V. V.; Volkov, Yu. O.; Dembo, K. A.; Kozhevnikov, I. V.; Roshchin, B. S.; Frolov, D. A.; Tikhonov, A. M. Condensation of Silica Nanoparticles on a Phospholipid Membrane. *JETP Lett.* **2011**, *94* (7), 585−587.

(40) Tikhonov, A. M. Multilayer of Phospholipid Membranes on a Hydrosol Substrate. *JETP Lett.* **2010**, *92*, 356−359.

(41) Asadchikov, V. E.; Babak, V. G.; Buzmakov, A. V.; Dorokhin, Yu. P.; Glaholev, I. P.; Zanevskii, Yu. V.; Zryuev, V. N.; Krivonosov, Y.; Mamich, V. F.; Moseiko, L. A.; Moseiko, N. I.; Mchedlichvili, B. V.; Savel'ev, S. V.; Senin, R. A.; Smykov, L. P.; Tudosi, G. A.; Fateev, V. D.; Chernenko, S. P.; Cheremukhina, G. A.; Shilin, Yu. N.; Shishkov, V. A.; et al. An X-ray Diffractometer with a Mobile Emitter-Detector System. *Instrum. Exp. Tech.* **2005**, *48* (3), 364−372.

(42) Hess, B.; Kutzner, C.; van der Spoel, D.; Lindahl, E. GROMACS 4: Algorithms for Highly Efficient, Load-Balanced, and Scalable Molecular Simulation. *J. Chem. Theory Comput.* **2008**, *4* (3), 435−447.

(43) Lucas, T. R.; Bauer, B. A.; Davis, J. E.; Patel, S. Molecular dynamics simulation of hydrated DPPC monolayers using charge equilibration force fields. *J. Comput. Chem.* **2012**, *33* (2), 141−152.

DOI: 10.1021/acs.langmuir.9b01450

(44) Michaud-Agrawal, N.; Denning, E. J.; Woolf, T. B.; Beckstein, O. MDAnalysis: a toolkit for the analysis of molecular dynamics simulations. *J. Comput. Chem.* **2011**, *32* (10), 2319−2327.

(45) Humphrey, W.; Dalke, A.; Schulten, K. VMD: visual molecular dynamics. *J. Mol. Graphics* **1996**, *14* (1), 33−38.

(46) Nesterenko, A. M.; Ermakov, Y. A. Moleculardynamic Simulation of Phospholipid Bilayers: Ion Distribution at the Surface of Neutral and Charged Bilayer in the Liquid Crystalline State. *Biochemistry (Moscow) Supplement Series A: Membrane and Cell Biology* **2012**, *6* (4), 320−328.

(47) Ermakov, Yu. A. Relationships between Electrostatic and Mechanical Characteristics of Dimyristoylphosphatidylserine Monolayer. *Biochemistry (Moscow) Supplement Series A: Membrane and Cell Biology* **2011**, *5* (4), 379−384.

(48) Sinha, S. K.; Sirota, E. B.; Garoff, S.; Stanley, H. B. X-ray and neutron scattering from rough surfaces. *Phys. Rev. B: Condens. Matter Mater. Phys.* **1988**, *38* (4), 2297−2312.

(49) Akin, F. A.; Jang, I.; Schlossman, M. L.; Sinnott, S. B.; Zajac, G.; Fuoco, E. R.; Wijesundara, M. B. J.; Li, M.; Tikhonov, A.; Pingali, S. V.; Wroble, A. T.; Hanley, L. Nanostructure of Fluorocarbon Films Deposited on Polystyrene from Hyperthermal C3F5+ Ions. *J. Phys. Chem. B* **2004**, *108* (28), 9656−9664.

(50) Pingali, S. V.; Takiue, T.; Luo, G.; Tikhonov, A. M.; Ikeda, N.; Aratono, M.; Schlossman, M. L. X-Ray Studies of Surfactant Ordering and Interfacial Phases at the Water-Oil Interface. *J. Dispersion Sci. Technol.* **2006**, *27*, 715−722.

(51) Tikhonov, A. M.; Schlossman, M. L. Vaporization and Layering of Alkanols at the Oil/Water Interface. *J. Phys.: Condens. Matter* **2007**, *19*, 375101.

(52) Tikhonov, A. M. Diffuse X-Ray Scattering near a Two-Dimensional Solid - Liquid Phase Transition at the n-Hexane - Water Interface. *JETP Lett.* **2016**, *104*, 309.

(53) Kozhevnikov, I. V. Physical analysis of the inverse problem of X-ray reflectometry. *Nucl. Instrum. Methods Phys. Res., Sect. A* **2003**, *508* (3), 519−541.

(54) Kozhevnikov, I. V.; Peverini, L.; Ziegler, E. Development of a self-consistent free-form approach for studying the three-dimensional morphology of a thin film. *Phys. Rev. B: Condens. Matter Mater. Phys.* **2012**, *85*, 125439.

(55) Buff, F. P.; Lovett, R. A.; Stillinger, F. H., Jr. Interfacial Density Profile for Fluids in the Critical Region. *Phys. Rev. Lett.* **1965**, *15* (15), 621−623.

(56) Mandelstam, L. Uber die Rauhigkeit freier Flussigkeitsoberflachen. *Ann. Phys.* **1913**, *346*, 609−624.

(57) Smoluchovsky, M. V. Molekular-kinetische Theorie der Opaleszens von Gasen im kritischen Zustande, sowie einiger verwandter Erscheinungen. *Ann. Phys.* **1908**, *330*, 205−226.

(58) Tikhonov, A. M.; Asadchikov, V. E.; Volkov, Yu. O.; Roshchin, B. S.; Honkimaki, V.; Blanco, M. V. Model-Independent X-Ray Scattering Study of a Silica Sol Surface. *JETP Lett.* **2018**, *107* (6), 384−389.

(59) Wang, X.; He, Q.; Zheng, S.; Brezesinski, G.; Mohwald, H.; Li, J. Structural Changes of Phospholipid Monolayers Caused by Coupling of Human Serum Albumin: A GIXD Study at the Air/Water Interface. *J. Phys. Chem. B* **2004**, *108*, 14171−14177.

(60) Helm, C. A.; Tippmann-Krayer, P.; Mohwald, H.; Als-Nielsen, J.; Kjaer, K. Phases of phosphatidyl ethanolamine monolayers studied by synchrotron x-ray scattering. *Biophys. J.* **1991**, *60* (6), 1457−1476.

(61) Aman, K.; Lindahl, E.; Edholm, O.; Hakansson, P.; Westlund, P.-O. Structure and Dynamics of Interfacial Water in an La Phase Lipid Bilayer from Molecular Dynamics Simulations. *Biophys. J.* **2003**, *84*, 102−115.

(62) Olzynska, A.; Zubek, M.; Roeselova, M.; Korchowiec, J.; Cwiklik, L. Mixed DPPC/POPC Monolayers: All-atom Molecular Dynamics Simulations and Langmuir Monolayer Experiments. *Biochim. Biophys. Acta, Biomembr.* **2016**, *1858* (12), 3120−3130.

(63) Schalke, M.; Losche, M. Structural models of lipid surface monolayers from X-ray and neutron reflectivity measurements. *Adv. Colloid Interface Sci.* **2000**, *88*, 243−274.

(64) Brockman, H. Dipole potential of lipid membranes. *Chem. Phys. Lipids* **1994**, *73* (1−2), 57−79.

(65) Miller, A.; Helm, C. A.; Mohwald, H. The colloidal nature of phospholipid monolayers. *J. Phys. (Paris)* **1987**, *48* (4), 693−701.

(66) Eisenberg, M.; Gresalfi, T.; Riccio, T.; McLaughlin, S. Adsorption of Monovalent Cations to Bilayer Membranes Containing Negative Phospholipids. *Biochemistry* **1979**, *18* (23), 5213−5223.

(67) Ermakov, Y. A. The determination of binding site density and association constants for monovalent cation adsorption onto liposomes made from mixtures of zwitterionic and charged lipids. *Biochim. Biophys. Acta, Biomembr.* **1990**, *1023* (1), 91−97.

(68) Pethica, B. A. Are electrostatic potentials between regions of different chemical composition measurable? The Gibbs−Guggenheim principle reconsidered, extended and its consequences revisited. *Phys. Chem. Chem. Phys.* **2007**, *9*, 6253−6262.

(69) Diaz, S.; Amalfa, F.; Lopez, A. C. B.; Disalvo, E. A. Effect of water polarized at the carbonyl groups of phosphatidylcholines on the dipole potential of lipid bilayers. *Langmuir* **1999**, *15*, 5179−5182.

(70) Wang, L. Measurements and Implications of the Membrane Dipole Potential. *Annu. Rev. Biochem.* **2012**, *81* (1), 615−635.

(71) Schneider, M. F.; Andelman, D.; Tanaka, M. Stripes of partially fluorinated alkyl chains: dipolar Langmuir monolayers. *J. Chem. Phys.* **2005**, *122* (9), 094717.

(72) Braslau, A.; Pershan, P. S.; Swislow, G.; Ocko, B. M.; Als-Nielsen, J. Capillary waves on the surface of simple liquids measured by x-ray reflectivity. *Phys. Rev. A: At., Mol., Opt. Phys.* **1988**, *38* (5), 2457−2473.

(73) Schwartz, D. K.; Schlossman, M. L.; Kawamoto, E. H.; Kellogg, G. J.; Pershan, P. S.; et al. Thermal diffuse x-ray-scattering studies of the water-vapor interface. *Phys. Rev. A: At., Mol., Opt. Phys.* **1990**, *41* (10), 5687−5690.

(74) Parratt, L. G. Surface Studies of Solids by Total Reflection of X-Rays. *Phys. Rev.* **1954**, *95* (4), 359−369.

(75) Small, D. M. *The Physical Chemistry of Lipids*; Plenum Press: New York, 1986.

DOI: 10.1021/acs.langmuir.9b01450
Langmuir 2019, 35, 12326−12338